



Effect of sensing distance of aluminum-coated FBG sensors installed on a composite plate under a low-velocity impact



Sang-Woo Kim

Department of Mechanical Engineering, Hankyong National University, Anseong-si, Gyeonggi-do 17579, Republic of Korea
Institute of Machine Convergence Technology, Hankyong National University, Anseong-si, Gyeonggi-do 17579, Republic of Korea

ARTICLE INFO

Article history:

Received 5 September 2016
Revised 10 October 2016
Accepted 17 October 2016
Available online 17 October 2016

Keywords:

Metal coating
Memory effect
Carbon fiber reinforced polymer composite
Impact behavior
Damage mechanics

ABSTRACT

This study investigates the effect of sensing distance on multiplexed aluminum-coated (Al-coated) fiber Bragg grating (FBG) sensors when they are applied to a carbon fiber reinforced polymer (CFRP) composite plate. The study involved a low-velocity impact test and its finite element analysis for the plate. The findings indicated that all the results from the test and FEA were consistent with each other. Additionally, the results revealed that permanently induced residual strains of all three Al-coated FBG sensors were linearly related to the sensing distance measured from the impact point. The findings also suggested that the linear relationship between the residual strains and sensing distances was closely related to the linear correlation between the sensing position and the maximum strains experienced by the composite plate. This implied that the impact information experienced by the composite structure could be quantitatively evaluated if the correlations between the structural deformation and residual strains with respect to the sensing distance were constructed in advance. Therefore, the correlation between the residual strains and the sensing distance examined in this study can improve the integrity of the proposed damage evaluation methodology and can be utilized as guidelines for designing a metal-coated optical fiber sensor (MCOFS) based damage evaluation systems for actual applications.

© 2016 Elsevier Ltd. All rights reserved.

1. Introduction

Fiber reinforced polymer (FRP) composites exhibit excellent mechanical properties such as high specific stiffness, high strength, and fatigue and corrosion resistance. This has led to their widespread use in many fields [3–6], especially in aerospace engineering [7,8]. However, composite structures are susceptible to damage from external impact loadings. Low-velocity impacts can cause impact-induced damage such as fiber breakage, matrix cracking, fiber-matrix debonding, and delamination. These damages are sometimes referred to as “barely visible impact damages (BVID)” because they cannot be visually inspected.

In the author’s previous studies [1,9,10], the author proposed a methodology using a metal-coated optical fiber sensor (MCOFS) to evaluate impact-induced damages of composite structures under low-velocity impacts and quasi-static indentation. Furthermore, Choi et al. [2] proposed aluminum (Al)-packaged Brillouin optical correlation domain analysis (BOCDA) sensors by using a similar approach. The BOCDA sensors were based on the Brillouin scatter-

ing effect [11–13], and it was demonstrated that Al-packaged OFS achieved a spatial resolution of 2 cm and could successfully produce residual strains of the sensors following the impact tests. These methodologies for damage evaluation and detection using MCOFS were based the “memory effects” of an elasto-plastic metal coated on the surface of optical fiber sensors. That is, the impact-induced damages could be assessed by measuring residual strain values since the maximum strains as well as the impact energy experienced by composite structures were correlated with the residual strain values [1,2,9,10,14]. This implied that the MCOFS could recall the information of the impact events that occurred in the past. This phenomenon is referred to as the “memory effects”. The methodology using MCOFS could be applied to the composite structures during operating periods and especially during inoperative periods.

However, previous laboratory tests for the proposed methodology were primarily conducted by focusing on the feasibility of the methodology under limited conditions [1,2,9,10,14–16]. This study builds on the previous feasibility studies and investigates the effect of the sensing distance of multiplexed Al-coated FBG sensors from the impact point. The sensing distance can be an important factor when the sensors are in operation because the mechanical

E-mail address: swkim@hknu.ac.kr

behaviors and responses of MCOFS can significantly vary according to the distance between an impact point and a sensing position. Additionally, prior to actual usage, it should be verified that the structural vibration induced by the external impact does not significantly affect the residual strain producing characteristics of the sensors with respect to the sensing distance. This ensures that the sensors are able to recollect the past impact information experienced by composite structures.

Fig. 1 shows a prime example of an actual application of MCOFS for damage evaluation of a composite cylinder. As shown in Fig. 1 (a), a distributed type of MCOFS was preferred for damage evaluation and detection because it covers a wide area range. Fig. 1(b) shows the actual application of an Al-packaged distributed sensor for the impact detection of a composite cylinder. However, the actual application of the MCOFS continues to be limited because the effect of the sensing distance on the residual strains is not well established. Thus, it is necessary to examine the sensing distance to understand how the residual strains induced by the metal coating should be varied with respect to the sensing distance prior to an actual application.

This study focused on a type of MCOFS, namely a multiplexed Al-coated fiber Bragg grating (FBG) sensor, in order to examine the effect of sensing distance. The reason for using multiplexed FBG sensors instead of distributed sensors was because the sensing capability of the former significantly exceeded that of the latter. Furthermore, a commercial interrogator system for FBG sensors provides excellent measurement resolution. Low-velocity impact tests for a composite plate with three Al-coated FBG sensors were performed to investigate the effect of sensing distance. The behavior of the composite plate with respect to the impacts was validated with the numerical results calculated by a finite element analysis (FEA) based on a continuum damage mechanics (CDM) considering damage model. The study also involved examining structural responses and strain distributions of the composite plate. Finally, the effect of the sensing position on the residual strains induced by three multiplexed Al-coated FBG sensors was investigated, and the relationship between the residual strains and sensing position was examined.

2. Metal-coated FBG sensors

Metal-coated FBG sensors permanently deform under alternately strained and unstrained state due to elasto-plastic metal coating. However, normal FBG sensors do not produce residual strains because they behave in a linear elastic manner. The principle of metal-coated FBG sensors is based on the shift of reflected wavelength satisfying the Bragg condition as given by the following equation:

$$\lambda_{\text{Bragg}} = 2n_e \Lambda_{\text{Bragg}}, \quad (1)$$

where λ_{Bragg} , Λ_{Bragg} , and n_e denote Bragg wavelength, period of the Bragg grating, and effective refractive index, respectively.

Fig. 2 illustrates the principle of metal-coated FBG sensors.

Under constant temperature conditions, the residual strain of metal-coated FBG sensors is estimated by measuring the wavelength shift as given by the following equation in accordance with previous studies [9,10,15,16]:

$$\varepsilon_r = \frac{1}{1 - P_e} \left(\frac{\lambda_r - \lambda_i}{\lambda_i} \right) = \frac{1}{1 - P_e} \left(\frac{\Delta\lambda_r}{\lambda_i} \right), \quad (2)$$

where $\Delta\lambda_r$, λ_i , λ_r , and P_e ($=0.22$) denote wavelength shift, initial wavelength, final wavelength shifted by permanent residual strain, and photo-elastic constant of an optical fiber, respectively.

FBG sensors recoated with ultraviolet (UV) curable acrylate and with Bragg gratings of 10 mm were used. An aluminum-alloy 1235-O foil with a thickness of 18 μm was used to coat the sensors using a cyanoacrylate adhesive. The details of the fabrication process are described in a previous study [1].

3. Experiment

3.1. A composite plate

A carbon fiber reinforced polymer (CFRP) composite plate was fabricated using a unidirectional prepreg (CU125NS; Hankook Fiber Co.) consisting of carbon fiber and epoxy resin. The prepreg was layered according to a layup sequence of

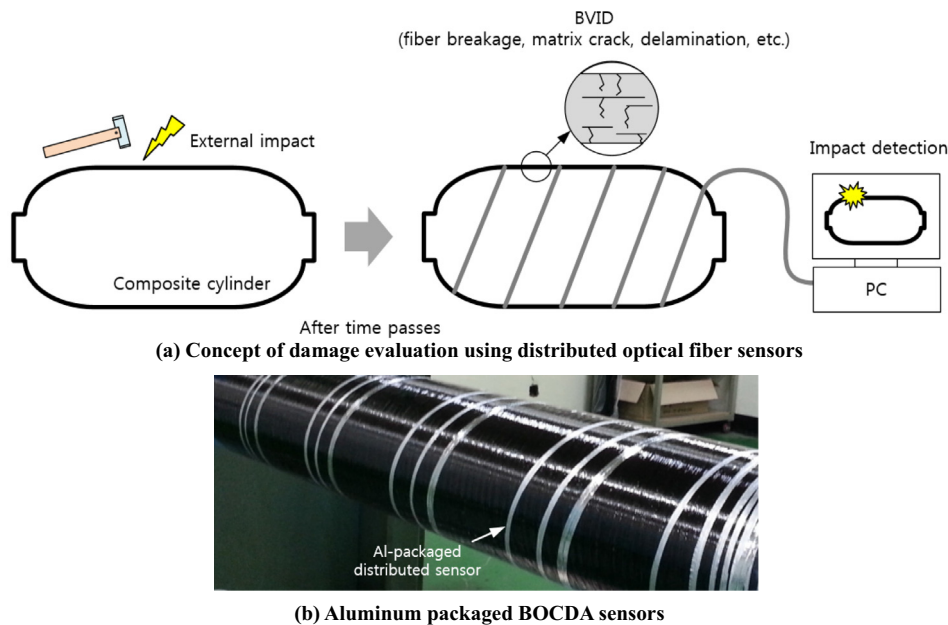


Fig. 1. Application of aluminum-coated optical fiber sensors.

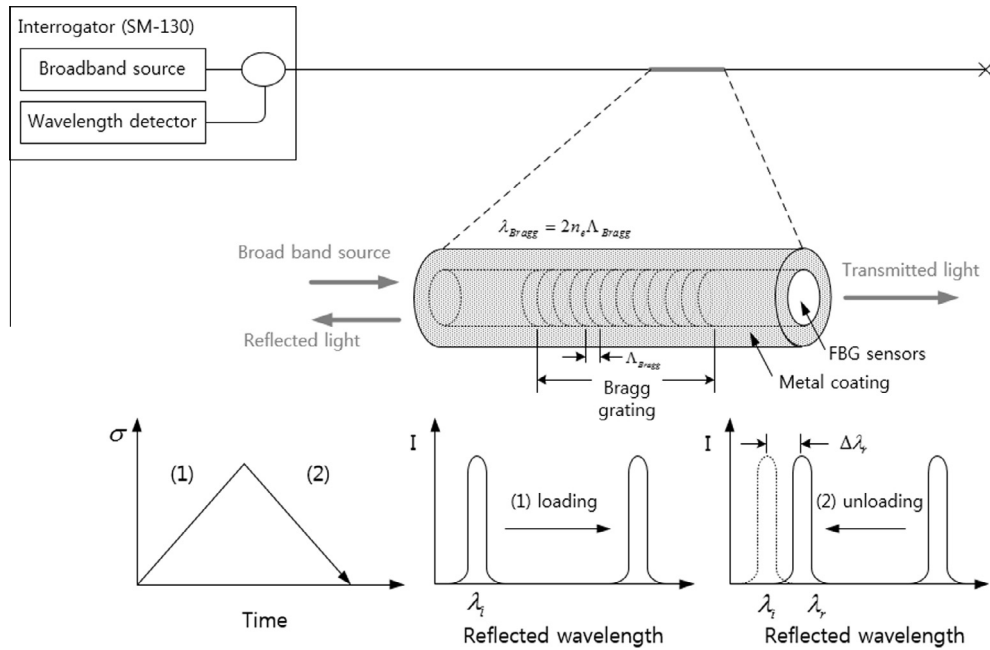


Fig. 2. Principle of metal-coated fiber Bragg grating sensors.

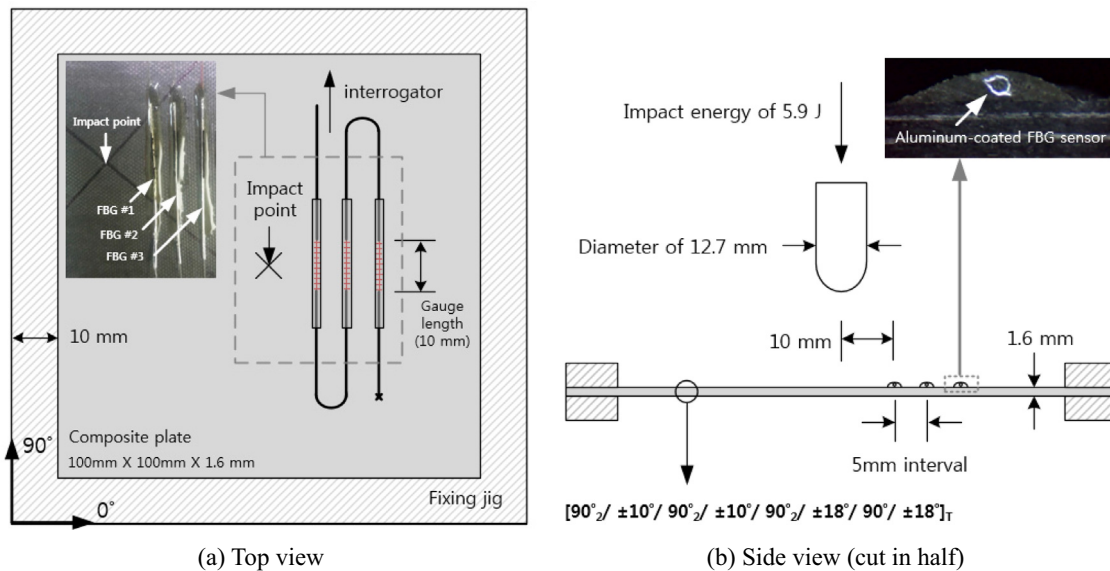
$[90^{\circ}_2/\pm 10^{\circ}/90^{\circ}_2/\pm 10^{\circ}/90^{\circ}_2/\pm 18^{\circ}/90^{\circ}/\pm 18^{\circ}]_T$, in accordance with a similar sequence used in a previous study [9]. It was cured in an autoclave under a pressure of 7 atm and a temperature of 130 °C for a period of 2 h. The dimensions of the composite plate were 100 mm × 100 mm, and its thickness was 1.6 mm. Three Al-coated FBG sensors were bonded on the surface of the plate by using an epoxy adhesive (Quick Set Auto Epoxy; Loctite Ltd.).

Fig. 3 shows a schematic diagram of the fabricated CFRP composite with three multiplexed Al-coated FBG sensors. Among the three Al-coated FBG sensors, FBG #1 was located at a distance of 10 mm from the impact point (i.e., the center of the plate) as shown in Fig. 3(b). The three sensors were installed at regular intervals of 5 mm in order to examine the effect of the sensing distance. Initial wavelengths of three FBG sensors, namely FBG#1, FBG#2, and FBG#3, were 1537.57 nm, 1547.52 nm, and

1557.41 nm, respectively. Two fixing jigs (an upper jig and a lower jig) with a width of 10 mm were used to secure the plate. Thus, the dimension of the test section of the plate was 80 mm × 80 mm. The impactor with a diameter of 12.5 mm is positioned at the center of the plate.

3.2. A low-velocity impact test

A low-velocity impact test was conducted on the CFRP composite plate mounted with three multiplexed Al-coated FBG sensors. The test was conducted by using a universal impact testing machine (Instron Daynatup 8250; INSTRON). An impact load with a target impact energy of 6 J (actually measured as 5.903 J) was applied at the center of the plate. As discussed in the next section, the external impact damages were not observed on the surface of



(a) Top view

(b) Side view (cut in half)

Fig. 3. A composite plate with multiplexed aluminum-coated fiber Bragg grating sensors.

the composite plate following the impact. However, the impact energy of 5.903 J was sufficient to create the internal damages, i.e., BVID. Therefore, a target impact energy of 6 J was considered as extremely suitable to examine the performance of MCOFSS because it could dramatically reduce the structural safety while maintaining the external conditions of the plate at normal conditions.

The strain data obtained from the sensors were measured with a sampling frequency of 1 kHz by using a commercial interrogation system (SM-130; Micron Optics Inc.). Specifically, the sampling frequency was not sufficient to measure the structural responses during the short impact time, which was less than 11 ms. However, it was sufficient to assess the quantity of the residual strain and structural responses following the impact for a long time. The final residual strains after the impact test were estimated based on the initial wavelength measured before fixing the plate because the metal-coated FBG sensors were naturally strained while fixing or unfixing the plate. That is, a small deformation of the plate also affected the quantity of residual strain of the sensors.

4. A finite element analysis for a low-velocity impact

A FEA based on the CDM was performed to validate a low-velocity impact test. A damage model proposed by Kim et al. [17,18] was applied to the FEA to numerically examine the impact behavior and damage propagation of the composite plate. In the CDM approach, the material properties, i.e., Young's modulus, shear modulus, and Poisson's ratio were assumed to be degraded by the extent of damage in the composite plate. The material property values are given by the following equations [17,18]:

$$E_i = d_i E_i^0, \quad G_{ij} = d_i G_{ij}^0, \quad \nu_{ij} = d_i \nu_{ij}^0, \quad (3)$$

where E_i , G_{ij} , ν_{ij} , and d_i denote the Young's modulus, shear modulus, Poisson's ratio, and degradation factor, respectively. The superscript, "0" indicates an initial material property without damage. In this study, a degradation factor characterized by a cumulative distribution function of two-parameter Weibull distribution (i.e., a shape parameter and a scale parameter) was used for material strength, as given by the following equation [17,18]:

$$d = e^{-(\sigma/\lambda)^m} = e^{\frac{1}{m} \ln \left[\frac{1}{1 + \frac{\sigma}{\lambda}} \right]^m} e^{(E^0 \varepsilon / \lambda)^m} \quad (4)$$

Eq. (4) represents the one-dimensional expression of the degradation factor of composites. The parameters, m and λ denote the shape parameter and scale parameter of the Weibull distribution, respectively. The other parameters, namely σ , ε , and $\Gamma(\cdot)$ denote the stress, strain, and gamma function, respectively. The damage parameters presented in previous studies [17] with respect to the damage modes of composites were used. These parameters were based on the damage criteria developed by Hashin et al. [19]. The cohesive zone model was applied to simulate inter-laminar damages. The FEA, considering the damage model, was performed

by using a commercial FE simulator ABAQUS/Explicit with a user defined subroutine code, VUMAT. The material properties used in the simulation are shown in Table 1 [9,17].

Fig. 4 shows the FE model for the CFRP composite plate including an impactor and two fixing jigs. The element type of C3D8R was applied to whole model except for the cohesive zone. The element type of COH3D8 was applied to the seven layers of the cohesive zone between lay-ups: 90°_2 and $\pm 10^\circ$, $\pm 10^\circ$ and 90°_2 and $\pm 10^\circ$, $\pm 10^\circ$ and 90°_2 and $\pm 18^\circ$, $\pm 18^\circ$ and 90°_2 and $\pm 18^\circ$. The total numbers of nodes and elements were 152,496 and 141,600, respectively. A lower jig was fixed while a pressure of 1 MPa suppressed an upper jig to replicate the clamping conditions. An impact velocity of 1.359 m/s was determined by reflecting an impact energy of 6 J and considering an impactor mass of 6.5 kg.

5. Results

5.1. A low-velocity impact test

5.1.1. Test validation

The impact behaviors of the composite plate are shown in Fig. 5. Contact force and central displacement history of the plate during the impact test are illustrated in Fig. 5(a) and (b), respectively. In the FE simulation, the maximum contact force and central displacement were slightly overestimated. The maximum contact force was measured as 2.977 kN and calculated as 3.096 kN, and the maximum central displacement was measured as 5.159 mm and calculated as 4.58 mm. These overestimations were induced by the difference of the impact energy between the test and FEA. Additionally, the overestimations were the result of decreased accurate clamping pressure during the simulation.

Specifically, the bending stiffness of the plate could increase if the clamping pressure on the upper jig increased, and this could thereby decrease the central displacement. The contact forces could contemporarily decrease because the damage to the plate around the impact point increased as the clamping pressure increased. Although the results obtained by the tests and the FEA showed slight differences, they were generally consistent irrespective of the clamping pressure and impact energy. Furthermore, the trends of the experimental and analytical results also showed good agreement. Therefore, this validated that the low-velocity impact test conducted in this study exhibited a good performance.

5.1.2. Impact-induced damages and structural responses

The impact-induced damages of the composite plate due to the low-velocity impact test were examined through FEA and visual inspection. Fig. 6 shows the impact induced damages of the composite plate. Fiber damages, matrix damages, and delamination of the plate are shown in Fig. 6(a)–(c), respectively. With respect to the fiber damages, the fibers of the plate did not fully fail because the impact energy of 6.0 J was not sufficient to break the fibers. However, some fibers near the impactor and lower surfaces of

Table 1
Material properties of CU125NS prepreg composite [9,17].

General properties		Weibull parameters			Cohesive properties	
Symbol	Value	Symbol	Scale Param. (λ)	Shape Param. (m)	Symbol	Value
E_{11}	116.0 GPa	X_T	2945 MPa	32.9	t_1	33 MPa
E_{22}, E_{33}	7.69 GPa	X_C	1650 MPa	14.6	t_2	54 MPa
G_{12}, G_{13}	4.92 GPa	Y_T	54 MPa	22.6	t_3	54 MPa
G_{23}	3.2 GPa	Y_C	240 MPa	10.5	G_{IC}	330 N/m
ν_{12}, ν_{13}	0.31	γ_{12}, γ_{13}	5%	1.3	G_{IIc}	800 N/m
ν_{23}	0.52	γ_{23}	5%	1.3	G_{IIIc}	800 N/m

Param. = Parameter; G_{IC} , G_{IIc} , G_{IIIc} = Fracture toughness for Mode I, II, III.

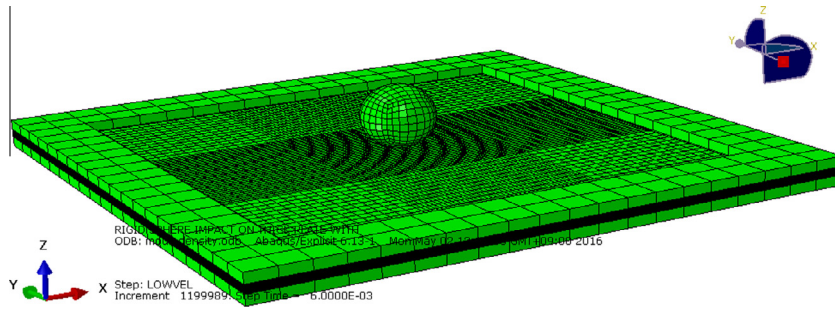
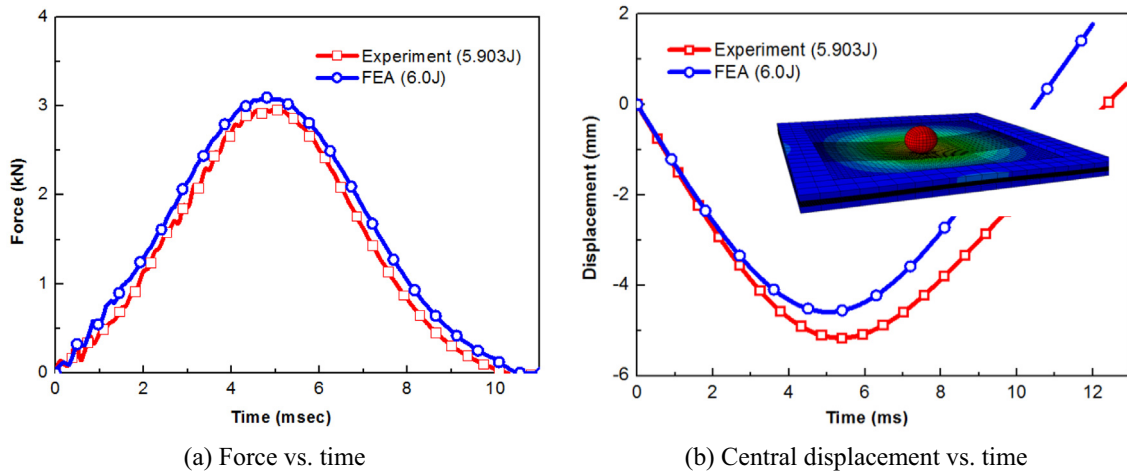


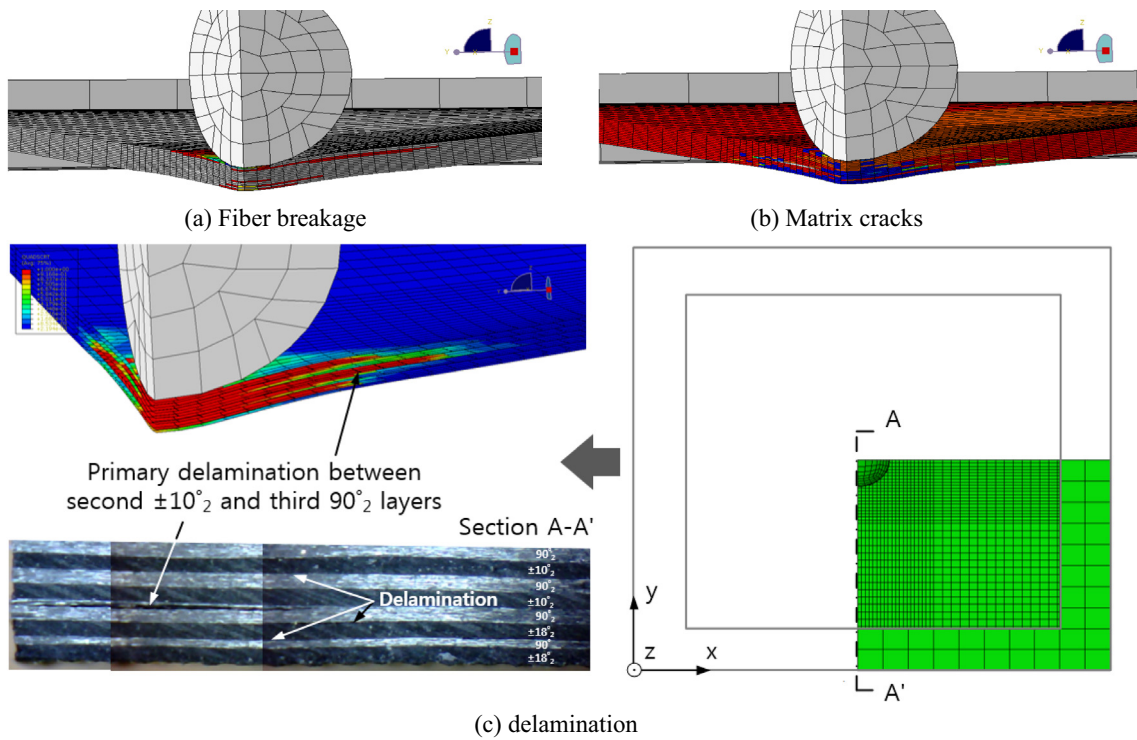
Fig. 4. A finite element model for a composite plate with an impactor and fixing jigs.



(a) Force vs. time

(b) Central displacement vs. time

Fig. 5. Force and displacement history during the impact.



(a) Fiber breakage

(b) Matrix cracks

(c) delamination

Fig. 6. Deflection and damages of a composite plate due to the impact.

the plate were locally subjected to tensile stress along the fiber direction due to the bending of the plate, and thus they were partially degraded. With respect to the matrix damages, the matrix right under the impactor was locally damaged due to the compressive stress generated by the impactor. Furthermore, the area in which matrix cracks appeared near the lower surface was larger than that in which matrix cracks appeared near the upper surface. With respect to the delamination, the cohesive zone model simulated the inter-lamina damages.

As shown in Fig. 6(c), the calculated area was compared to the delamination observed in the composite plate cut in half. With respect to the FEA, the delaminations were simulated at the interfaces between the first $\pm 10^\circ$ and second 90°_2 layers, second $\pm 10^\circ$ and third 90°_2 layers, and first $\pm 18^\circ$ and first 90° layers. They corresponded to the delamination position estimated by the test. Among the delaminations, the primary delaminations between the second $\pm 10^\circ$ and third 90°_2 layers near the neutral axis were clearly observed in both results. It was reasonable to assume that the delamination occurred between two layers with different fiber directions. The maximum lengths of the delaminations evaluated by the test and the FEA were 7.10 mm and 7.6 mm, respectively.

Fig. 7 shows the structural responses of a composite plate. Fig. 7(a) shows the strain responses measured from three multiplexed Al-coated FBG sensors, and Fig. 7(b) depicts the calculated maximum strain distribution near the sensing position of the sensors. As shown in Fig. 7(a), the initial strains for the three sensors were not zero. Specifically, the strains for FBG #1, FBG #2, and FBG #3 were -0.0021% , -0.029% , and -0.01% , respectively.

The initial wavelengths for calculating the strains were recorded prior to fixing the plate. This indicated that the plate was slightly deformed when the plate was fixed on an impact test machine. That is, three FBG sensors with an inherent strain were operated during the test. Significant vibrations occurred right after the impact test, and they were measured by the three FBG sensors. The vibrations with compressive strains were mainly observed. This phenomenon indicated that the vibration modes with a convex shape were suppressed by the clamping condition and impact direction. The vibration induced by an impact load could be detrimental for the damage evaluation capability of the sensors. It is necessary for the multiplexed sensors to recollect the maximum strains experienced by the plate irrespective of the vibration to accurately evaluate impact-induced damages. Following the disappearance of the vibrations, the strains for the three sensors converged to -0.053% , -0.058% , and -0.030% , respectively. These values did not show tendencies or correlations with the sensing

distance. However, the Al-coated FBG sensors could recall the structural deformations experienced by the plate in the past. Additionally, the sensors could recall the maximum strains by producing the residual strains with a particular tendency. As discussed in the next section, although the sensors experienced severe vibrations after impact, the residual strains measured after removing the plate from the fixing jigs indicated an increased tendency with respect to the sensing distance. Then, the impact information could be inferred from the inverse of the residual strains.

As shown in Fig. 7(b), the present study examined the calculated maximum strains along the plate instead of the maximum strains measured in experimental tests because the sampling rate of the commercial interrogator used in the test was not sufficient to accurately measure the maximum strain at the moment of impact. All the maximum strains measured from the FBG sensors were negative. The negative values of strains were reasonable given the static deformation of the plate. The tensile stress was generated in the vertical direction of the FBG sensors on the plate, while the compressive stress occurred in the longitudinal direction of the sensors due to the deflection of the plate with a concave shape. As illustrated in Fig. 7(b), a maximum strain values experienced by the plate in the sensing field was correlated with the sensing distance. Hence, the maximum strain values showed a linearly increasing tendency, and the strain values were 0.509% , 0.440% , and 0.355% for FBG #1, FBG #2, and FBG #3, respectively. As discussed in the next section, the increasing tendency and the linear relationship with respect to the sensing distance were very important in quantitatively estimating the impact information.

In the large deformation field, the maximum strains radically decreased as they approached the center of the plate. This occurred due to the local reduction of bending stiffness of the plate generated by the impact-induced damages as illustrated in Fig. 6. The sensors could be indirectly damaged by large external strains when they were installed at the large deformation field. For example, the interface between the UV curable acrylate coating and metal coating could be debonded. The impactor could also directly break the sensors because an external impact could occur at any arbitrary position during the actual application. Then, the impact position could be clearly evaluated because the destruction of the sensor could easily signal the impact position.

5.2. Effect of sensing distance on residual strains

The wavelength changes for three multiplexed Al-coated FBG sensors and their final residual strains are shown in Fig. 8. The light

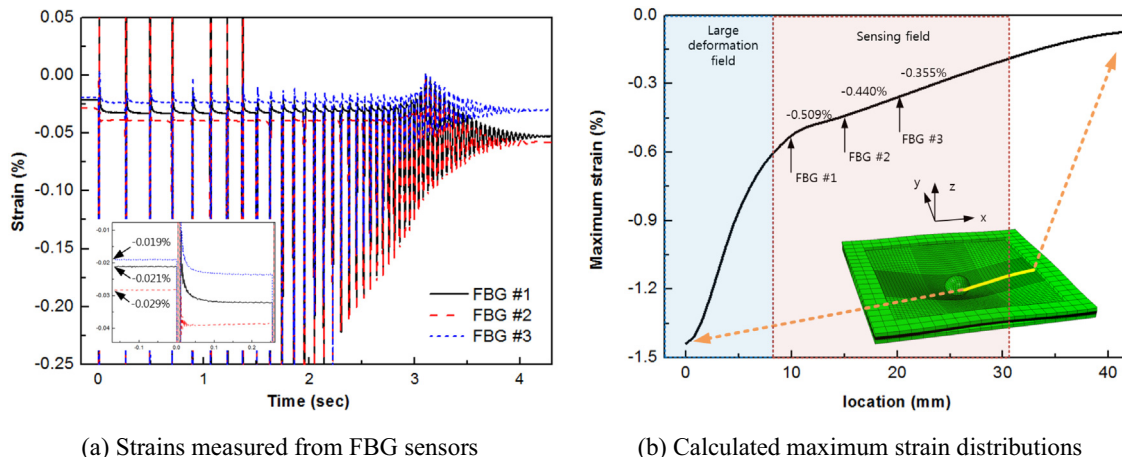


Fig. 7. Structural responses of a composite plate.

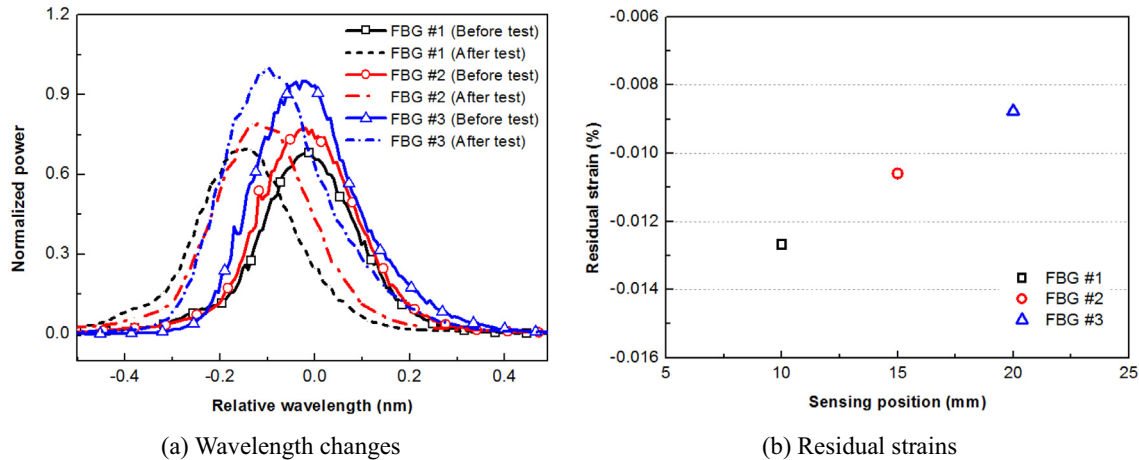


Fig. 8. Wavelength changes and residual strains of multiplexed aluminum-coated FBG sensors.

spectra of relative wavelengths for the three multiplexed Al-coated FBG sensors are presented in Fig. 8(a). The initial peak values for the sensors were recorded prior to the clamping of the plate by the fixing jigs. The peaks with values equivalent to residual strains were permanently moved to the left. The signal characteristics of the three sensors were not distorted during the test although they were subjected to impact loadings and severe vibrations. This implied that the three sensors were properly positioned and resistant to vibrations.

The residual strains induced by the three multiplexed Al-coated FBG sensors are presented in Fig. 8(b). They were recorded after removing the plate from the fixing jigs. The quantity of the residual strains of the three sensors linearly increased as the sensing distance from the impact point increased. Notably, the maximum strains of the three FBG sensors were also linearly related to the sensing distance, as mentioned in Section 5.1.2. This could be because the three multiplexed Al-coated FBG sensors did not forget the impact information (i.e., the maximum strains) during the test despite experiencing severe vibrations. That is, the sensors recalled the impact information experienced by the plate in the past. With respect to the actual application, the increase in the amount of residual strains as the impact point was approached was extremely essential to damage evaluation because impact information such as the impact point, impact energy, and strain levels could be quantitatively assessed by the referring residual strains according to the sensing distance. This implied that the impact information experienced by the composite structure could be quantitatively evaluated if the correlations among the structural deformation and residual strains according to the sensing distance were constructed in advance.

6. Conclusion

In this study, a low-velocity impact test for a composite plate was performed to investigate the effect of the sensing distance of three multiplexed Al-coated FBG sensors. The results obtained from the FEA based on CDM approach were compared to that of the experimental tests to validate the impact behaviors of the plate. All the results from the experimental tests and the simulation were consistent with each another. The permanently induced residual strains of the three multiplexed Al-coated FBG sensors were linearly related to the sensing distance from the impact point despite the sensors experiencing severe vibrations after the impact. This mean that some residual strain linearly increased as the impact point was approached. The results indicated that the

linear relationship between the residual strain values and sensing distance was closely related to the linear correlation between the sensing position and the maximum strains experienced by the composite plate. This suggested that the impact information experienced by the composite structure could be quantitatively evaluated if the correlations between the structural deformation and residual strains with respect to the sensing distance were constructed in advance. Therefore, the correlation between the residual strains and the sensing distance of three multiplexed Al-coated FBG sensors examined in this study could improve the integrity of the proposed damage evaluation methodology. Furthermore, the results of this study could be utilized as guidelines for designing MCOFS based damage evaluation systems for actual applications.

Acknowledgements

This research was supported by Basic Science Research Program through the National Research Foundation of Korea (NRF) funded by the Ministry of Science, ICT & Future Planning (2016R1C1B2010417).

References

- [1] Kim SW, Jeong MS, Lee I, Kim EH, Kwon IB, Hwang TK. Determination of the maximum stresses experienced by composite structures using metal coated optical fiber sensors. *Compos Sci Technol* 2013;78:48–55.
- [2] Choi BH, Kwon IB. Residual strain sensor using Al-packaged optical fiber and Brillouin optical correlation domain analysis. *Opt Express* 2015;23(5):6867–77.
- [3] Fuchs ERH, Field FR, Roth R, Kirchain RE. Strategic materials selection in the automobile body: economic opportunities for polymer composite design. *Compos Sci Technol* 2008;68(9):1989–2002.
- [4] Bakis CE, Bank LC, Brown VL, Cosenza E, Davalos JF, Lesko JJ. Fiber reinforced polymer composites for construction: state of the art review. *J Compos Constr* 2002;6(2):73–87.
- [5] Brøndsted P, Lilholt H, Lystrup A. Composite materials for wind turbine blades. *Annu Rev Mater Res* 2005;35:505–38.
- [6] Rajapakse YDS, Hui D. Marine composites and sandwich structures. *Compos Part B Eng* 2008;39(1):1–4.
- [7] Baker AA, Dutton S, Kelly D. *Composite materials for aircraft structures*. AIAA Education Series; 2004.
- [8] Ghoshal A, Ayers J, Gurvich M, Urban M, Bordick N. Experimental investigations in embedded sensing of composite components in aerospace vehicles. *Compos Part B Eng* 2015;71:52–62.
- [9] Kim SW, Cha MC, Lee I, Kim EH, Kwon IB, Hwang TK. Damage evaluation and strain monitoring of composite plates using metal-coated FBG sensors under quasi-static indentation. *Compos Part B Eng* 2014;66:36–45.
- [10] Kim SW, Kim EH, Jeong MS, Lee I. Damage evaluation and strain monitoring for composite cylinders using tin-coated FBG sensors under low-velocity impacts. *Compos Part B Eng* 2015;74:13–22.

- [11] Bao X, DeMerchant M, Brown A, Bremner T. Tensile and compressive strain measurement in the lab and field with the distributed Brillouin scattering sensor. *J Lightwave Technol* 2001;19(11):1698–704.
- [12] Hotate K, Hasegawa T. Measurement of Brillouin gain spectrum distribution along an optical fiber using a correlation-based technique—proposal, experiment and simulation. *IEICE Trans Electron* 2000;E83-C(3):405–12.
- [13] Yoon HJ, Song KY, Kim HM, Kim JS. Strain monitoring of composite steel girder bridge using distributed optical fibre sensor system. *Procedia Eng* 2011;10:2544–7.
- [14] Im JE, Kim MH, Choi KS, Kwon IB, Hwang TK. Aluminum-thin-film packaged fiber Bragg grating probes for monitoring the maximum tensile strain of composite materials. *Appl Opt* 2014;53:3615–20.
- [15] Kim SW, Jeong MS, Lee I, Kwon IB, Hwang TK. Effects of mechanical and geometric properties of adhesive layer on performance of metal-coated optical fiber sensors. *Int J Adhes Adhes* 2013;47:1–12.
- [16] Kim SW, Jeong MS, Lee I, Kwon IB. Static mechanical characteristics of tin-coated fiber Bragg grating sensors. *Sens Actuators A Phys* 2014;214:156–62.
- [17] Kim EH, Rim MS, Lee I, Hwang TK. Composite damage model based on continuum damage mechanics and low velocity impact analysis of composite plates. *Compos Struct* 2013;95:123–34.
- [18] Kim EH, Lee I, Hwang TK. Low-velocity impact and residual burst-pressure analysis of cylindrical composite pressure vessels. *AIAA J* 2012;50(10):2180–93.
- [19] Hashin Z. Failure criteria for unidirectional fiber composites. *J Appl Mech* 1980;47(2):329–34.